www.czasopisma.pan.pl PAN www.journals.pan.pl

ARCHIVES of FOUNDRY ENGINEERING

ISSN (2299-2944)
Volume 21
Issue 2/2021

65 – 69

9/2

10.24425/afe.2021.136099

Published quarterly as the organ of the Foundry Commission of the Polish Academy of Sciences

Formation Mechanism for the TiN–MnS Complex Inclusions in Tire Cord Steel

Jialiu Lei *, Xiumin Wang, Dongnan Zhao, Yongjun Fu
Hubei Polytechnic University, China
* Corresponding author: Email address: leijialiu@hbpu.edu.cn

Received 13.01.2021; accepted in revised form 17.05.2021

Abstract

High strength tire cord steel is extensively used in radial ply tyres as the framework material, but the presence of brittle single titanium inclusions or complex titanium inclusions can cause failure of the wires and jeopardize their performance in production. In order to provide a key guidance on the control of titanium inclusions, it is necessary to clarify their formation mechanism during solidification. In the present work, the thermodynamic calculations were employed for an elaboration on their formation mechanism, combined with the industrial test. The TiN–MnS complex inclusions observed by SEM−EDS shows that the internal corresponds to TiN and the external is MnS. Thermodynamic calculations based on the microsegregation model indicate that MnS forms first, which can act as a nucleation site for the co–deposit of TiN in the mushy zone. As the MnS inclusions have a better deformation than that of TiN inclusions, then the TiN inclusions are wrapped by the MnS inclusions, generating TiN–MnS complex inclusions after rolling.

Keywords: Thermodynamic calculations, Formation mechanism, TiN–MnS complex inclusions, Tire cord steel

1. Introduction

Titanium is a kind of common microalloying addition in molten steels to improve mechanical properties of final products *via* the grain refinement during hot rolling and to stabilize the alloy against sensitization to intergranular corrosion [1–4]. However, low titanium content is demanded for special steel production, such as high strength tire cord steel. It is desirable to control the precipitation of Ti inclusions during tire cord steel production.

As a superior quality product of wire rod, tire cord steel is extensively used in radial ply tyres as the framework material due to its characteristics of high strength and good toughness. Before tire cord steels are made, steel wires are drawn from φ 5.5 to φ 0.15 mm in diameter and subjected to cyclic stress in the drawing and twisting process [5, 6]. Therefore, the breakage during fabrication is a crucial issue, and this is especially sensitive with the existence of angular and non-deformable Ti inclusions, such as TiN or Ti(CN) for high strength steels [7–9], this causes the decrease of fatigue property and affects the traffic safety seriously. In recent years, with the increasing demand for outstanding performance of steel wire, the control of titanium inclusion is becoming more and more stringent.

In order to effective control the Ti inclusions, it is necessary to clarify their formation mechanism in tire cord steel. To date, the precipitation and growth behavior of pure TiN inclusions have been reported before in tire cord steel [10–12]. But apart from the pure TiN inclusions, the TiN–MnS complex inclusions were also observed, and their formation mechanism remained unclear. For an elaboration on their formation mechanism, the thermodynamic calculations were employed combined with the industrial test in this paper.

2. Experimental Aspects

The following process is adopted for the production of high

strength tire cord steel: basic oxygen furnace (BOF)→tapping→ ladle furnace (LF)→soft blowing (SB)→continuous casting (CC) →rolling, as shown in Fig. 1.

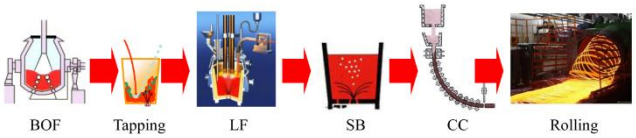

Fig. 1. Production process of tire cord steel

During the tapping, ferromanganese (Fe–Mn) and ferrosilicon (Fe–Si) were employed for the deoxidation alloying, and SiC was employed to deoxidize the refining slag. After LF refining, the removal of inclusions by soft blowing about 25 min was done. Finally, the liquid steel was sent to the continuous casting (CC) platform. The steel specimens taken from the wire rod with 20 mm in diameter after rolling and drawing were investigated by a Scanning Electron Microscope equipped with an Energy Dispersive Spectrometer (SEM–EDS). The C and S content were analyzed by a carbon–sulfur analyzer (CS–8800), the O and N were analyzed by a oxygen–nitrogen analyzer (LECO–TC500), and the content of other elements were analyzed by ICP–AES analyzer. The chemical composition was shown in Table 1, and Als is the acid-soluble aluminum in steek bulk.

Table 1.
Chemical composition of the wire rod (wt%)

C	Si	Mn	S	P	Als	Ti	N	O
0.80	0.18	0.52	0.0072	0.0179	0.0012	0.0011	0.0041	0.0016

3. Results and Discussion

3.1 Morphology of Complex Ti Inclusions

The TiN–MnS complex inclusions observed in wire rod by SEM–EDS was given in Fig. 2. The area scanning analysis of the complex inclusion shows that, the morphology of MnS inclusion exhibits irregular shape and TiN inclusion shows a square shape with sharp edges and corners. It indicates that the internal corresponds to TiN and the external is MnS.

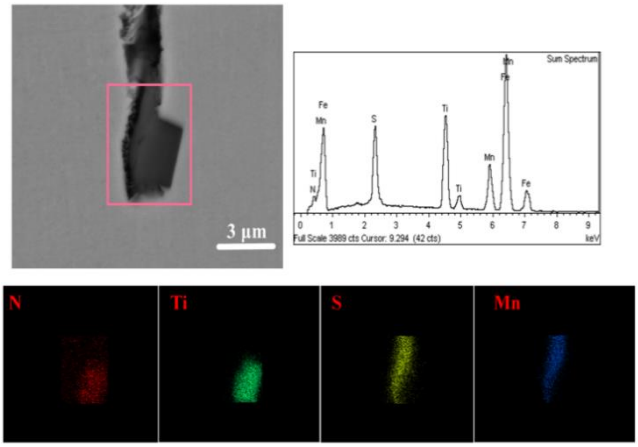

Fig. 2. TiN inclusion wrapped by MnS in wire rod

3.2 Thermodynamic Analysis

To provide a better clarity of the generation of TiN and MnS, the liquidus and solidus temperatures together with the thermodynamic data of the solutes involved should be acquired. According to the chemical constituents of the steel, the solidus and liquidus temperatures can be obtained as follows [13, 14].

$$T_L = 1809 - \sum m_i C_{0,i} \tag{1}$$

$$T_s = 1809 - \sum n_i C_{0,i} \tag{2}$$

where T_L and T_S are the liquidus and solidus temperatures (K), respectively, $C_{0,i}$ is the initial mass percentage of solute element i (wt%), m_i and n_i are the liquidus and solidus slope of solute element i (K/%). The values of m_i and n_i are listed in Table 2.

Table 2.
The liquidus and solidus slope of solute element (K/%)

Item	C	Si	Mn	S	P	Al	Ti	N	O
m_i	65	8	5	25	30	3	20	90	80
n_i	175	20	30	575	280	7.5	40	--	160

The thermodynamic calculation for the generation of TiN and MnS inclusions in tire cord steel are given as follows [15, 16].

$$[\mathrm{Ti}] + [\mathrm{N}] = \mathrm{TiN}_{(\mathrm{inc})}$$
$$\log K_{\mathrm{TiN}} = \log \frac{a_{\mathrm{TiN}}}{a_{\mathrm{Ti}} \cdot a_{\mathrm{N}}} = \log \frac{a_{\mathrm{TiN}}}{f_{\mathrm{Ti}}[\%\mathrm{Ti}] \cdot f_{\mathrm{N}}[\%\mathrm{N}]} = \frac{15217}{T} - 5.643 \tag{3}$$

$$[\mathrm{Mn}] + [\mathrm{S}] = \mathrm{MnS}_{(\mathrm{inc})}$$
$$\log K_{\mathrm{MnS}} = \log \frac{a_{\mathrm{MnS}}}{a_{\mathrm{Mn}} \cdot a_{\mathrm{S}}} = \log \frac{a_{\mathrm{MnS}}}{f_{\mathrm{Mn}}[\%\mathrm{Mn}] \cdot f_{\mathrm{S}}[\%\mathrm{S}]} = \frac{8630}{T} - 4.747 \tag{4}$$

where $\log K$ represents the logarithm of equilibrium constant; T is the absolute temperature (K); a denotes the activity, for pure inclusions the activity is equal to 1; f_i is the Henrian activity

coefficient of component i relative to the dilute solution, which can be calculated by Equation (5), and e_i^j is the interaction coefficients, which are given in Table 3 [13, 17, 18].

$$\log f_i(1873\ \mathrm{K}) = \sum e_i^j [\%j] \tag{5}$$

Table 3.
Interaction coefficients in liquid steel at 1873 K

e_i^j	C	Si	Mn	P	S	Al	O	N	Ti
N	0.13	0.047	-0.021	0.045	0.007	-0.028	0.05	0	-0.537
Ti	-0.165	0.056	0.0043	-0.064	-0.11	0.12	-1.8	-1.8	0.013
Mn	-0.07	-0.0002	0	-0.0035	-0.048	0.07	-0.083	-0.091	0.019
S	0.112	0.063	-0.026	0.029	-0.028	0.035	-0.27	0.01	-0.072
S	0.112	0.063	-0.026	0.029	-0.028	0.035	-0.27	0.01	-0.072

The effect of temperature on activity coefficients (f) is given by the following equations [19–21]:

$$\log f_{\mathrm{N}}(T) = (\frac{3280}{T} - 0.75)\log f_{\mathrm{N}}(1873\ \mathrm{K}) \tag{6}$$

$$\log f_{\mathrm{Ti}}(T) = (\frac{2557}{T} - 0.365)\log f_{\mathrm{Ti}}(1873\ \mathrm{K}) \tag{7}$$

$$\log f_{\mathrm{Mn}}(T) = (\frac{2538}{T} - 0.355)\log f_{\mathrm{Ti}}(1873\ \mathrm{K}) \tag{8}$$

$$\log f_{\mathrm{S}}(T) = (\frac{2538}{T} - 0.355)\log f_{\mathrm{Ti}}(1873\ \mathrm{K}) \tag{9}$$

According to the formulas (1)–(9), the demanded concentration products for the formation of TiN and MnS inclusions in liquid steel are given in Fig. 3 and Fig. 4, respectively. It is obvious that the demanded equilibrium concentration of N, Ti, S, and Mn for the generation of TiN and MnS inclusions cannot get in liquid phase or mushy zone based on the thermodynamic calculation results. In actual steel compositions, the TiN or MnS inclusions would precipitate in the solid region, only when the temperature is lower than 1380.94 K or 1211.83 K, respectively.

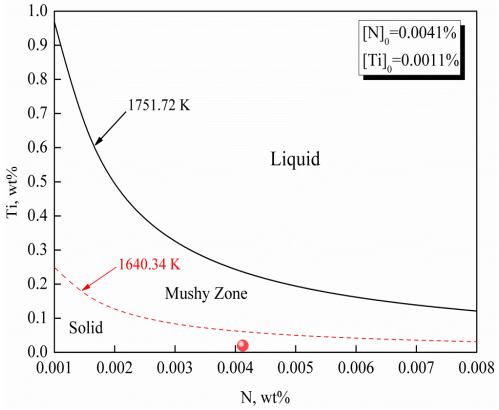

Fig. 3. Demanded concentration products for TiN inclusions

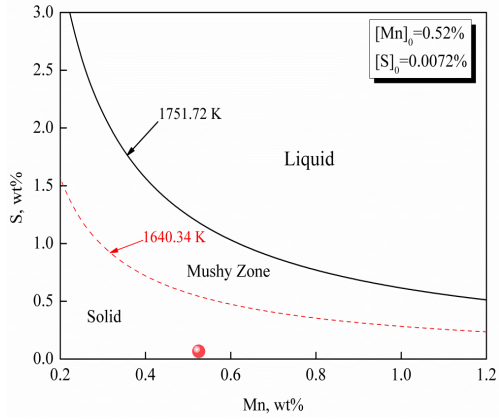

Fig. 4. Demanded concentration products for MnS inclusions

However, the preceding analytical results are obtained with hypothesis that the compositions are homogeneous. As solidification continues, the redistribution of solute atoms results in microsegregation because of the different diffusion rates between liquid and solid phases. The actual concentration of solutes during coagulation process change because of microsegregation, and then the TiN or MnS inclusions have the chance to precipitate. The segregation of solutes in micro–regions can be expressed by the following formulas [22, 23].

$$\mathrm{C_{L,i}} = \mathrm{C_{0,i}}(1\text{-}(1\text{-}\beta_i \mathrm{k_i})\mathrm{g})^{(\mathrm{k_i}\text{-}1)/(1\text{-}\beta_i \mathrm{k_i})} \tag{10}$$

There into,

$$\beta_i = \frac{2\alpha_i}{1+2\alpha_i} \tag{11}$$

$$\alpha_i = \frac{2D_{S,i}\tau}{(\lambda_{\mathrm{SDAS}}/2)^2} \tag{12}$$

where $C_{L,i}$ is the actual mass concentration of solute element i (wt%), k_i represents the balanced distribution coefficient between solid and liquid phases, g denotes the solid fraction, $D_{S,i}$ is the diffusion rate in solid phase (cm^2/s), λ_{SDAS} represents the secondary dendrite arm spacing (μm), β_i is the back-diffusion parameters, α_i is the Fourier series of solute element i, and τ represents the local solidification time (min).
The solid-liquid interface temperature T_{L-S}, can be obtained by equation (13) [24].

$$T_{L-S} = T_M - \frac{T_M - T_L}{1 - g\frac{T_L - T_S}{T_M - T_S}} \tag{13}$$

where T_M denotes the melting point of pure iron. λ_{SDAS} and τ are given by equations (14) and (15), respectively [25].

$$\lambda_{\mathrm{SDAS}} = 143.9 R_c^{-0.3616} C_{0,\mathrm{C}}^{(0.5501 - 1.996 C_{0,\mathrm{C}})} \ (C_{0,\mathrm{C}} > 0.15\%) \tag{14}$$

$$\tau = \frac{T_L - T_S}{R_c} \tag{15}$$

where R_c represents the cooling speed, which was set as 300 K/min

according to the actual production process, and the balanced distribution coefficients and diffusion rates are shown in Table 4 [26], where R is the ideal gas constant, whose value is 8.314 J/(mol·K). According to Fe–C phase diagram, the solidification of tire cord steel with 0.80 wt% carbon is in Austenite (γ).

Table 4.
Balanced distribution coefficients and diffusion rates

Element	$k^{\gamma/L}$	$D_\gamma, \mathrm{cm}^2/\mathrm{s}$
N	0.48	$0.91\exp(-168490/RT)$
Ti	0.33	$0.15\exp(-250956/RT)$
S	0.035	$2.4\exp(-223426/RT)$
Mn	0.785	$0.055\exp(-249366/RT)$

According the formulas, the balanced activity product log K and actual activity product log Q of TiN and MnS can be represented as follows.

$$\log K_{\mathrm{TiN}} = 5.643 - \frac{15217}{T}, \log Q_{\mathrm{TiN}} = \log\left(f_{\mathrm{N}} \cdot [\%\mathrm{N}] \cdot f_{\mathrm{Ti}} \cdot [\%\mathrm{Ti}]\right) \quad (16)$$

$$\log K_{\mathrm{MnS}} = 4.747 - \frac{8630}{T}, \log Q_{\mathrm{MnS}} = \log\left(f_{\mathrm{S}} \cdot [\%\mathrm{S}] \cdot f_{\mathrm{Mn}} \cdot [\%\mathrm{Mn}]\right) \quad (17)$$

When the actual activity product $\log Q$ exceeds the balanced activity product $\log K$, the TiN or MnS inclusions begin to precipitate and grow.

3.3 Calculation Results and Discussion

Combining the above equations with the compositions, the generation of TiN or MnS inclusions in liquid steel during coagulation process is obtained in Fig. 5.

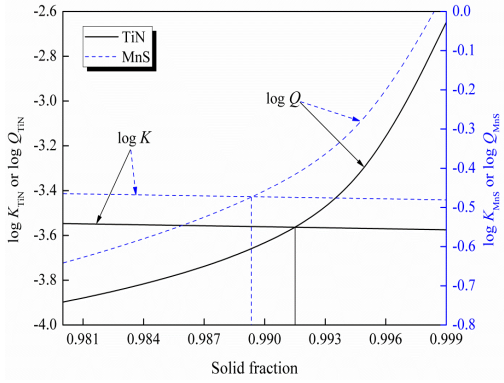

Fig. 5. Calculation results for the precipitation of TiN and MnS

Fig. 5 indicates that TiN and MnS can precipitate during solidification when solid fraction is greater than 0.9915 and 0.9894, respectively. It shows that the MnS forms prior to that of TiN, due to the fact that the TiN and MnS have the same cubic crystal structure, and similar low index surfaces lattice constant (as shown in Table 5), the MnS can act as a nucleation site for the co–deposite of TiN.

Table 5.
Parameter for the crystal structure of TiN and MnS

Inclusion	Crystal system	Space group	Lattice parameter (Å)
TiN	Cubic–NaCl	FM-3M	4.241 [27]
MnS	Cubic–NaCl	FM-3M	5.223 [27]

Therefore, the MnS can be acted as the substrate and TiN as the nucleation, resulting in heterogeneous nucleation on the MnS inclusions. The possible formation mechanism can be summarized as follows: MnS and TiN are precipitated in austenite during solidification. MnS inclusion forms first depleting the surrounding zone from Mn and S, the decrease in Mn and S enhances the activity coefficient of N and Ti since the interaction parameters $e_{\mathrm{Ti}}^{\mathrm{S}}$ and $e_{\mathrm{N}}^{\mathrm{Mn}}$ are negative (as shown in Table 3), and then accelerates the precipitation of TiN inclusion as the temperature goes down. Since MnS and TiN have the same crystal structure, they tend to form together as complex ones. As the MnS inclusions have a better deformation than that of TiN inclusions, then the TiN inclusions can be wrapped by the MnS inclusions, forming the TiN–MnS complex inclusions in the wire rod after rolling, and exhibit the morphology shown in Fig. 2. The diagrammatic drawing of generating process for TiN–MnS complex inclusions is described in Fig. 6.

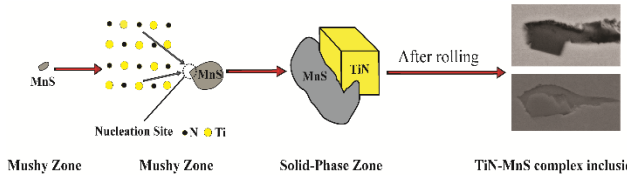

Fig. 6. Schematic diagram of formation mechanism for TiN–MnS complex inclusions

4. Summary

The TiN–MnS complex inclusions were observed in the wire rod by SEM. The area scanning analysis shows that, the morphology of MnS inclusion exhibits irregular shape and TiN inclusion shows a square shape with sharp edges and corners, indicating that the internal corresponds to TiN and the external is MnS.

At concentrations of N, Ti, S, and Mn in the tire cord steel, the required equilibrium concentrations for the formation of TiN and MnS inclusions cannot get in liquid phase or mushy zone.

Thermodynamic calculations based on the microsegregation model indicate that the MnS occurs prior to that of TiN, which can act as a nucleation site for the co–deposite of TiN. Due to the better deformation of MnS inclusion, the TiN inclusion can be wrapped by the MnS inclusion, forming TiN–MnS complex inclusion in the wire rod after rolling.

Acknowledgments

The authors would like to thank the National Natural Science Foundation of China (Grant No. 51704105).

References

[1] Abushosha, R., Vipond, R. & Mintz, B. (1991). Influence of titanium on hot ductility of as cast steels. *Materials Science & Technology*. 7(7), 613-621.

[2] Chen, Z., Li, M., Wang, X., He, S. & Wang, Q. (2019). Mechanism of floater formation in the mold during continuous casting of Ti-stabilized austenitic stainless steels. *Metals*. 9, 635-649.

[3] Karmakar, A., Kundu, S., Roy, S., Neogy, S., Srivastava, D. & Chakrabarti, D. (2014). Effect of microalloying elements on austenite grain growth in Nb–Ti and Nb–V steels. *Materials science and Technology*. 30(6), 653-664.

[4] Reyes-Calderón, F., Mejía, I., Boulaajaj, A. & Cabrera, J.M. (2013). Effect of microalloying elements (Nb, V and Ti) on the hot flow behavior of high–Mn austenitic twinning induced plasticity (TWIP) steel. *Materials Science and Engineering: A*. 560, 552-560.

[5] Chen, C.Y., Jiang, Z.H., Li, Y., Zheng, L.C., Huang, X.F. & Yang, G. (2019). State of the art in the control of inclusions in tire cord steels and saw wire steels–A Review. *Steel Research International*. 6, 1-13.

[6] Lei, J.L., Zhao, D.N., Fu, Y.J., & Xu, X.F. (2019). Research on the characterization of Ti inclusions and their precipitation behavior in tire cord steel. *Archives of Foundry Engineering*. 19(3), 33-37.

[7] Cui, H.Z. & Chen, W. Q. (2012). Effect of boron on morphology of inclusions in tire cord steel. *Journal of Iron and Steel Research International*. 19(4), 22-27.

[8] Wu, S., Liu, Z., Zhou, X., Yang, H. & Wang, G. (2017). Precipitation behavior of Ti in high strength steels. *Journal of Central South University*. 24(12), 2767-2772.

[9] Petit, J., Sarrazin-Baudoux, C. & Lorenzi, F. (2010). Fatigue crack propagation in thin wires of ultrahigh strength steels. *Procedia Engineering*. 2, 2317-2326.

[10] Liu, H.Y., Wang, H.L., Li, L., Zheng, J.Q., Li, Y.H. & Zeng, X.Y. (2011). Investigation of Ti inclusions in wire cord steel. *Ironmaking and Steelmaking*. 38(1), 53-58.

[11] Cai, X.F., Bao, Y.P., Wang, M., Lin, L., Dai, N.C. & Gu, C. (2015). 69Investigation of precipitation and growth behavior of Ti inclusions in tire cord steel. *Metallurgical Research and Technology*. 112(4), 407-418.

[12] Lei, J.L., Xue, Z.L., Jiang, Y.D., Zhang, J. & Zhu, T.T. (2012). Study on TiN precipitation during solidification for hypereutectoid tire cord steel. *Metalurgia International*. 17(9), 10-15.

[13] Chen, J.X. (2010). Common charts and databook for steelmaking. (2nd ed.). Beijing: Metallurgical Industry Press.

[14] Clyne, T.W., Wolf, M. & Kurz, W. (1982). The effect of melt composition on solidification cracking of steel with particular reference to continuous casting. *Metallurgical and Materials Transactions B*. 13(2), 259-266.

[15] Wada, H., & Pehlke, R.D. (1985). Nitrogen solubility and nitride formation in austenitic Fe–Ti alloys. *Metallurgical and Materials Transactions B*. 16(4), 815-822.

[16] Ma, Z., & Janke, D. (1998). Characteristics of oxide precipitation and growth during solidification of deoxidized steel. *ISIJ International*. 38(1), 46-52.

[17] Darken, L.S. (1967). Thermodynamics of binary metallic solutions. *Transaction of American Institute of Mining, Metallurgical, and Petroleum Engineers*. 239(1), 80-89.

[18] Yoshikawa, T., & Morita, K. (2007). Influence of alloying elements on the thermodynamic properties of titanium in molten steel. *Metallurgical and Materials Transactions B*. 38(4), 671-680.

[19] Kim, W., Jo, J., Chung, T., Kim, D. & Pak, J. (2007). Thermodynamics of titanium, nitrogen and TiN formation in liquid iron. *ISIJ International*. 47(8), 1082-1089.

[20] Ma, W.J., Bao, Y.P., Zhao, L.H., & Wang, M. (2014). Control of the precipitation of TiN inclusions in gear steels. *International Journal of Minerals Metallurgy and Materials*. 21(3), 234-239.

[21] Huang, X.H. (2001). *Theory of Iron and Steel Metallurgy*. (3rd ed.). Beijing: Metallurgical Industry Press.

[22] Won, Y.M. & Thomas, B.G. (2011). Simple model of micro–segregation during solidification of steels. *Metallurgical and Materials Transactions A*. 32(7), 1755-1767.

[23] Ohnaka, I. (1986). Mathematical-analysis of solute redistribution during solidification with diffusion in solid–phase. *ISIJ International*. 26(12), 1045-1051.

[24] Maugis, P. & Gouné, M. (2005). Kinetics of vanadium carbonitride precipitation in steel: a computer model. *Acta Materialia*. 53(12), 3359-3367.

[25] Manohar, P.A., Dunne, D.P., Chandra, T. & Killmore, C.R. (2007). Grain growth predictions in microalloyed steels. *ISIJ International*, 36(2), 194-200.

[26] Choudhary, S.K. & Ghosh, A. (2009). Mathematical model for prediction of composition of inclusions formed during solidification of liquid steel. *ISIJ International*. 49(12), 1819-1827.

[27] Gao, S., Wang, M., Guo, J.L., Wang, H. & Bao, Y.P. (2019). Extraction, distribution, and precipitation mechanism of TiN–MnS complex inclusions in Al-killed titanium alloyed interstitial free steel. *Metals and Materials International*. 12, 1-9.